Surface Plasmon Resonance (SPR) Electron and Energy Transfer in Noble Metal– Zinc Oxide Composite Nanocrystals

ARTICLE *in* THE JOURNAL OF PHYSICAL CHEMISTRY C · JULY 2008

Impact Factor: 4.77 · DOI: 10.1021/jp8018809

5 AUTHORS, INCLUDING:

Taewoo Kim
Seoul National University
273 PUBLICATIONS **1,842** CITATIONS
SEE PROFILE

Yun-Mo Sung
Korea University
107 PUBLICATIONS **1,641** CITATIONS
SEE PROFILE

Surface Plasmon Resonance (SPR) Electron and Energy Transfer in Noble Metal−Zinc Oxide Composite Nanocrystals

Myung-Ki Lee,[†] Tae Geun Kim,[‡] Woong Kim,*[,†] and Yun-Mo Sung*[,†]

Department of Materials Science and Engineering and Department of Electronic Engineering, Korea University, Seoul 136-713, South Korea

Received: March 03, 2008; Revised Manuscript Received: April 15, 2008

Au- and Ag-ZnO composite nanocrystals having a dumbbell-like structure were successfully synthesized through the nucleation and decomposition of zinc hydroxide at the surface of pre-existing Au and Ag nanoparticles, respectively. The average size of the Au and Ag nanoparticles used was ∼4 nm and that of the ZnO nanocrystals was ∼10 nm. The composite nanocrystals show strong crystallinity of face-centered cubic and wurztite structures from Au or Ag and ZnO, respectively. The composite nanocrystals show enhanced UV light emission due not only to the surface electron transfer from the Au or Ag to the ZnO by the surface plasmon resonance (SPR) but also to the extension of the Fermi energy level to the ZnO. The Au-ZnO composite nanocrystals showed significantly suppressed visible light luminescence, while the Ag-ZnO did not show any apparent difference compared to the ZnO nanocrystals.

1. Introduction

Over the past several years, semiconductor nanocrystals, especially II−VI groups, have attracted a great deal of attention due to their peculiar optical properties based on the so-called quantum confinement effect.[1–3] Most research on nanocrystals has converged to obtain modulated band gap emission or improved luminescence efficiency of nanometer-sized semiconductors mostly for optical applications such as light emitting diode (LED), laser diode (LD), and photosensors.[4–8] Recently, these applications have been rapidly expanding to biomedical and environmental fields such as luminescence cell tagging, drug delivery, chemical sensors, catalysts, and photovoltaics.[9–11] ZnO is a wide energy band gap II−VI semiconductor (3.37 eV) absorbing and emitting UV-light (∼368 nm), and its excitation binding energy is 60 meV, which provides ZnO material with high potential for applications in high-efficiency LED and high-density LD devices.[12–14] Compared to the bulk or thin film form, ZnO nanocrystals can achieve higher sensitivity and efficiency due to the increase of surface area to volume ratio, which is beneficial to light absorption/emission or electron transfer.

Nanometer-scale noble metals have been intensively studied, since they show unique light absorption characteristics when they are smaller than the wavelength of the incident light beam. The oscillation of high-density free electrons occurs under the irradiation of light, which is called surface plasmon resonance (SPR). Owing to the optical properties, they are finding various applications in photosensors and biomedical sensors. Also, recently SPR-based noble metal semiconductor nanocomposites have become a popular research topic because of the improved optical properties of the semiconductor.[15–17] It has been reported that the SPR electron and energy transfer from the metal surface to the surrounding semiconductor materials significantly modify their optical properties.[18–21] In this study, Au- and Ag-ZnO composite nanocrystals with an average Au and Ag size of ∼4 nm and an average ZnO size of ∼10 nm were successfully synthesized using wet chemical approaches. The photoluminescence (PL) properties of the composite nanocrystals were compared to previous research,[15–17] and the mechanism was discussed in detail based upon the SPR and the energy band structure.

2. Experimental Section

2.1. Preparation of Au and Ag Nanocrystals. The gold nanoparticles were prepared according to the procedure described by Murphy et al.[22] and the silver nanoparticles were prepared with minor modification. For the gold nanoparticles, an aqueous solution (20 mL) containing 2.5 mM $HAuCl_4 \cdot 3H_2O$ (99.9+%, Aldrich) and 2.5 mM trisodium citrate (from Riedel) was prepared in a flask. Next, 0.1 M $NaBH_4$ (99%, Aldrich) cold solution (0.6 mL) freshly prepared was added to the solution with stirring for 2−5 h. The solution turned pink immediately after adding $NaBH_4$, indicating nanoparticle formation. For the Ag nanoparticle preparation, $AgC_2H_3O_2$ (99%, Aldrich) was used as a precursor, and the whole synthesis procedure was exactly identical to the Au procedure except the evaporation of acetone above 80 °C for 2 h. When the $NaBH_4$ solution was added, the color of the solution containing Ag precursor turned yellow.

2.2. Preparation of Au- and Ag-ZnO Nanocomposites. The 0.05 M $Zn(NO_3)_2 \cdot 6H_2O$ (98%, Aldrich) in ethanol solution (4 mL) was mixed with the nanoparticle-containing solution. Then, 4 mL ethanol solution containing 0.025 M NaOH was added all at once and vigorously stirred for 1 h. White purple and white yellow suspensions were obtained and centrifuged to get the Au- and Ag-ZnO composite nanoparticles, respectively.

2.3. Characterizations of Au- and Ag-ZnO Nanocomposites. The crystal structure of the nanocomposites was measured by X-ray diffractometer (XRD, Rigaku Ultima 2000, $\lambda = 1.5418$ Å). The size and the morphology of the nanocomposites were determined using high-resolution transmission electron microscopy (HRTEM, FEI Technai G2 F30, 300 kV). For HRTEM sample preparation, a carbon-coated copper grid was placed on a filter paper and the nanocomposite suspended solution was

* To whom correspondence should be addressed. E-mail addresses: Woong Kim, woongkim@korea.ac.kr; Yun-Mo Sung, ymsung@korea.ac.kr. Tel: 82-2-3290-3286. Fax: 82-2-928-3584.
[†] Department of Materials Science and Engineering.
[‡] Department of Electronic Engineering.

10.1021/jp8018809 CCC: $40.75
Published on Web 06/14/2008

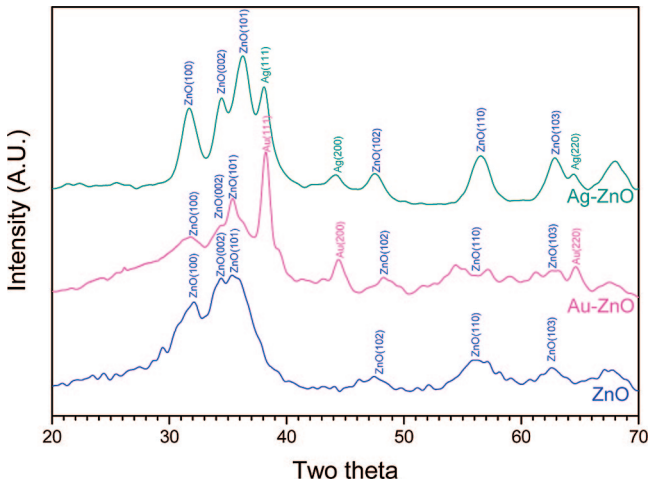

Figure 1. X-ray diffraction (XRD) patterns for ZnO, Au-ZnO, and Ag-ZnO nanocrystals.

dropped onto it using a syringe and air-dried for one day. The photoluminescence was measured by luminescence spectrometry (Aminco Bowman ±, Thermo electron corporation) using a 1 × 1 cm^2 area and 4 cm height quartz cuvette having transparent faces.

3. Results and Discussion

3.1. Morphology and Structure of Nanocomposites. Figure 1 shows X-ray diffraction (XRD) patterns of the Au-ZnO, Ag-ZnO, and ZnO nanostructures, respectively. The appearance of Au (111), (200) (JCPDS No. 01−1174), Ag (111), (200) (JCPDS No. 01−1164), and ZnO (100), (101) (JCPDS No. 05−0664) peaks confirms that crystalline Au, Ag, and ZnO phases are formed in Au- and Ag-ZnO nanocomposites, respectively. According to the Scherrer formula using the full width at half-maximum (fwhm), the size of Au and Ag nanoparticles was estimated at ∼4.5 nm and that of ZnO was ∼9 nm.

High-resolution transmission electron microscopy (HRTEM) images of Au- and Ag-ZnO nanocomposites in Figure 2 show that they are a dumbbell-like structure with an average size of ∼4 and ∼10 nm for the noble metals and the ZnO, respectively, which is in good agreement with the XRD results. The HRTEM images of Au-ZnO present the interplanar *d*-spacing of Au (111) and ZnO (100) atomic planes as ∼0.24 and ∼0.28 nm, respectively. Also, HRTEM images of Ag-ZnO show the interplanar *d*-spacing very close to that of Au-ZnO. The selected area electron diffraction (SAED) ring patterns clearly show the crystallinity of FCC metal and wurtzite ZnO phases. The reason that the noble metal-ZnO systems do not form a core/shell structure despite a small lattice parameter difference between Au and ZnO could lie in the difference in the crystalline structure between them, i.e., Au is cubic and ZnO is hexagonal. Due to the crystal structure mismatch, the interfacial energy would be too large, and thus to reduce the total free energy of the system, the dumbbell-like structure could form instead. The epitaxial nucleation and growth of the ZnO shell at the surface of Au was not observed in this study.

3.2. Synthesis of Au- and Ag-ZnO Nanocomposites. The formation mechanism of Au- and Ag-ZnO composites was speculated based on the nucleation and growth of ZnO at the surface of Au and Ag nanoparticles through the reduction of zinc ions to zinc hydride and its subsequent decomposition to ZnO. The possible routes for ZnO formation on the Au or Ag can be expressed as follows:[23,24]

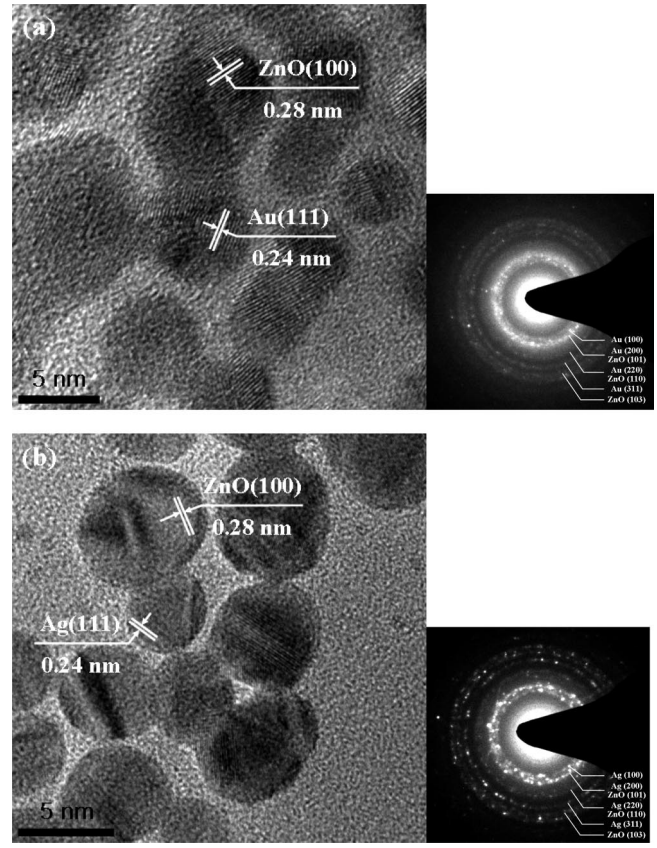

Figure 2. High-resolution transmission electron microscope (HRTEM) images and selected area diffraction (SAED) patterns of (a) Au-ZnO and (b) Ag-ZnO composite nanocrystals.

$$Zn(NO_3)_2 \cdot 6H_2O + 2NaOH \rightarrow Zn(OH)_2(gel) + 2NaNO_3 + 6H_2O \quad (1)$$

$$Zn(OH)_2(gel) + 2H_2O \rightarrow Zn^{2+} + 2OH^- + 2H_2O \rightarrow Zn(OH)_4^{2-} + 2H^+ \quad (2)$$

$$Zn(OH)_4^{2-} \rightarrow ZnO + H_2O + 2OH^- \quad (3)$$

In detail, the $Zn(NO)_3$ precursor is decomposed to Zn^{2+} ions in an aqueous solution and it is subsequently reduced to $Zn(OH)_2$ in the solution. In this process, the color of the solution changes from pink to light purple and light yellow. The Au or Ag nanoparticles supply the nucleation sites for the $Zn(OH)_2$, and the $Zn(OH)_2$ becomes $Zn(OH)_4^{2-}$ ions by further reaction with water. Finally, the $Zn(OH)_4^{2-}$ ions can be decomposed to ZnO, and the Au- or Ag-ZnO composite nanocrystals form. Due to the crystalline lattice mismatch between the Au or Ag (FCC) and ZnO (HCP), core/shell structures could not form, and instead the dumbbell-like structures formed in this study. The formation mechanism of the Au- or Ag-ZnO composite nanocrystals is depicted in Figure 3.

3.3. Optical Property of Au- and Ag-ZnO Nanocomposites. The photoluminescence (PL) characteristics of the nanocrystals are presented in Figure 4. The PL spectra of each sample are composed of two emission bands in the UV/visible range under the above band-edge excitation, which come from the ZnO component. In the case of ZnO materials, the UV-range emission, called radiative recombination, occurs due to recombination between the electrons in a conduction band and the holes in a valence band. On the other hand, the visible-range emission, called nonradiative recombination, occurs due to the

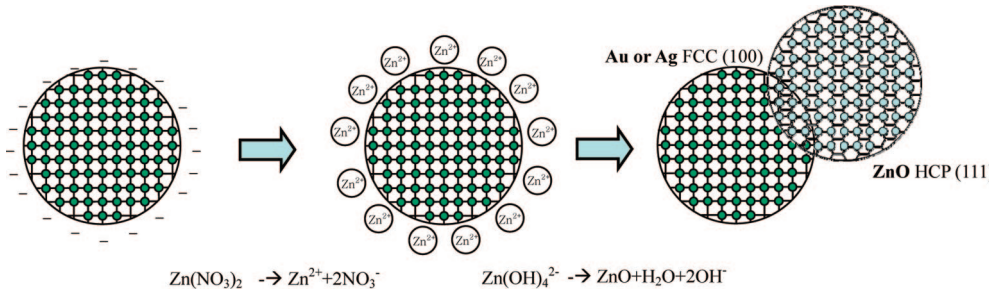

Figure 3. A suggested mechanism for the formation of Au- and Ag-ZnO nanocrystals by solution-phase synthesis.

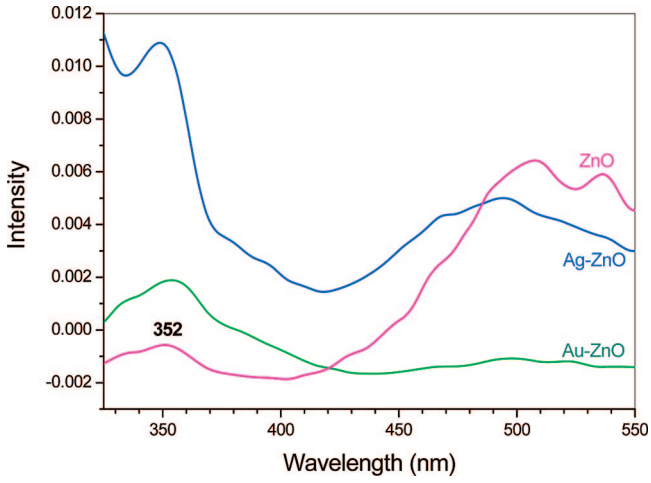

Figure 4. Photoluminescence (PL) spectra of ZnO, Au-ZnO, and Ag-ZnO nanocrystals.

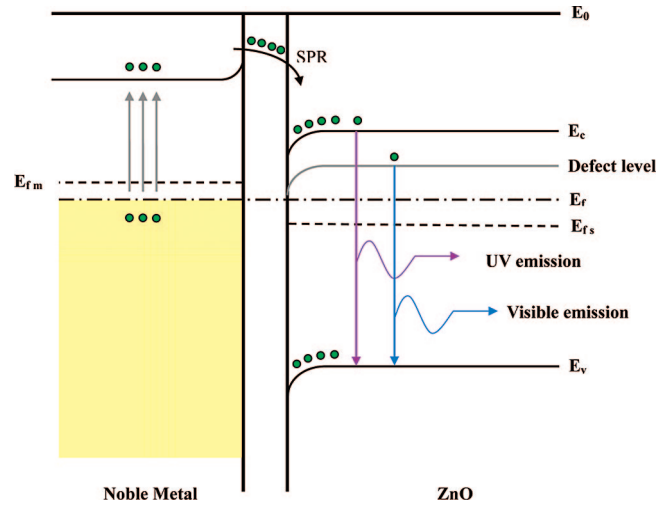

Figure 5. The energy band structure of a noble metal and ZnO showing the uniform Fermi energy level, induced by electron transfer between the metal and ZnO.

recombination between the electrons in a deep defect level or a shallow surface defect level and the holes in a valence band.[25,26] Therefore, the narrow UV emission band centered at 352 nm in Figure 4 is ascribed to the radiative recombination occurring in the ZnO. However, each sample shows a noticeable difference in the UV light emission intensity due to the distinct surface plasmon resonance (SPR) effect of the nanoscale noble metals. Under the irradiation of incident light having a wavelength larger than the particle size, the high-density electrons of the noble metal nanoparticles form an electron cloud and oscillate. If the noble metal nanoparticles are combined with ZnO, the electrons accumulate at the interface between the metal and the ZnO, leading to the downward band bending of the ZnO side and thus to the easy electron transfer from the Au or Ag nanoparticles to the ZnO side. Figure 5 shows the band bending, Fermi energy level of the ZnO, and electron transfer from the Au or Ag to the ZnO. Furthermore, the Au- and Ag-ZnO composite nanocrystals show different UV light emission intensity, since a noble metal has its own optical properties such as refractive index.[25] According to Rayleigh theory, the scattering light intensity is given by[27,28]

$$I = \frac{16\pi^4 a^6 n_{med}^4 I_0}{r^2 \lambda_0^4} \left| \frac{m^2 - 1}{m^2 + 2} \right|^2 \sin^2(\alpha) \qquad (4)$$

The relative refractive index m of a particle at a given wavelength may be a complex number which can be described as

$$m = \frac{(n_{rel} + i n_{im})}{n_{med}} \qquad (5)$$

Here, n_{rel} and n_{im} are the real and imaginary refractive indices of a material, respectively, presenting scattering and absorption of light in vacuum. The n_{rel} is higher than the n_{im} in the UV range, and the difference between the two indices is larger in Ag than in Au.[24] This implies that, in the UV range, Ag nanoparticles have larger m^2 values in eq 5, and thus Ag has higher light scattering intensity (I) than Au in eq 4. When the light scattering is stronger than absorption, the efficiency of the electron transfer from metal to semiconductor becomes high. Thus, the UV-light emission intensity of the Ag-ZnO composite nanocrystals becomes much higher than that of the ZnO and Au-ZnO. There must be reduction in the light emission due to the defected interfacial region existing between the Ag (Au) and ZnO nanpoarticles, possibly coming from the large (~17%) lattice mismatch. However, the interfacial region seems to supply routes for the effective electron transfer from Ag (Au) to ZnO since the PL intensity dominantly increases in both Au-ZnO and Ag-ZnO systems compared to ZnO.

On the other hand, in the visible range there exists broad light emission from the ZnO component. The mechanism of this broad visible-range emission is still under debate, and for example, Vanheusden et al.[25] explain that the visible emission is ascribed to the nonradiative recombination of holes with the electrons occupied by the ionized oxygen vacancies in ZnO.[26] Furthermore, Dijken et al.[29] describe that it is due to the nonradiative recombination between deep-level holes trapped in oxygen vacancy centers (V_O) and shallow-level electrons. Thus, these oxygen vacancies are generally accepted as responsible for the broad visible-range emission in ZnO. By considering energy band structures in the Au- or Ag-ZnO composite nanocrystal system, it can be concluded that the transfer of metal surface electrons to ZnO causes an increase of electron density in the conduction band of the ZnO. Furthermore, since the

emitted visible light photon energy of the ZnO nanocrystals matches the SPR energy of a metal, the emitted photons produce the SPR through energy transfer, which promotes the electrons in metal to an excited state by surface plasmon waves. The excited electrons will tunnel to the conduction band of the ZnO nanocrystals. On the basis of this mechanism, the opposite case can be considered to explain the decrease in the visible-range light emission in the Au- or Ag-ZnO composite nanocrystals. The electrons in the defect level of ZnO can be easily excited to the conduction band by the SPR energy transfer from a metal so that the probability of recombination between the trapped electrons and the holes decreases. Therefore, the visible emission of the Au- or Ag-ZnO composite nanocrystals is lower than that of the pure ZnO nanocrystals. The energy band structure of the noble metal-ZnO is also depicted in Figure 5. The Au-ZnO samples have almost negligible visible-range light emission most probably due to light absorption through the SPR of Au nanoparticles. Since the maximum SPR occurs at ~530 nm in Au nanoparticles, the visible-range light emitted from the ZnO nanocrystals can be considerably absorbed by the Au nanoparticles. One the other hand, the Ag-ZnO composite nanocrystals show broad visible-range light emission, and the PL intensity in the visible range is only slightly different from that of the pure ZnO nanocrystals. Since the maximum SPR occurs at ~400−420 nm in Ag nanoparticles, the visible light emitted from the ZnO nanocrystals is not substantially absorbed by the Ag nanoparticles as in the case with Au-ZnO composite nanocrystals.

4. Conclusions

In this study, Au- and Ag-ZnO composite nanocrystals were successfully synthesized using reduction of zinc ions and decomposition of zinc hydroxide at the surface of pre-existing Au or Ag nanoparticles. The composite nanocrystals are in a dumbbell-like shape, composed of ~4 nm Au or Ag in FCC and ~10 nm ZnO in wurtzite. It is found that the Ag-ZnO nanocrystals show very high PL intensity at a low wavelength range, compared to Au. Since Ag has a higher refractive index, it can cause a strong light scattering effect to the ZnO. The visible-range light (green) emission from the ZnO nanocrystals was considerably suppressed due to the SPR of Au in Au-ZnO composite nanocrystals, while it remained unchanged in Ag-ZnO composite nanocrystals since the SPR maximum of Ag nanoparticles is ~400−420 nm.

Acknowledgment. This work was supported by the Korea Research Foundation (KRF) Grant by the Korean Government (MOEHRD) (KRF-2006-311-D00568).

References and Notes

(1) Colvun, V. L.; Schlamp, M. C.; Alivisatos, A. P. *Nature* **1994**, *370*, 354.

(2) Sung, Y. M.; Lee, Y. J.; Park, K. S. *J. Am. Chem. Soc.* **2006**, *128*, 9003.

(3) Kwak, W. C.; Sung, Y. M.; Kim, T. G.; Chae, W. S. *Appl. Phys. Lett.* **2007**, *90*, 173111.

(4) Artemyev, M. V.; Woggon, U; Wannemacher, R.; Jaschinski, H; Langbein, W *Nano Lett* **2001**, *1*, 309.

(5) Hsu, J. P.; Tian, Z. R.; Simmons, N. C.; Matzke, C. M.; Voigt, J. A.; Liu, J. *Nano Lett.* **2005**, *5*, 83.

(6) Walker, G. W.; Sundar, V. C.; Rudzinski, C. M.; Wun, A. W. *Appl. Phys. Lett.* **2003**, *83*, 3555.

(7) Dabbousi, B. O.; Rodriguez-Viejo, J.; Mikulec, F. V.; Heine, J. R.; Mattoussi, H.; Ober, R.; Jensen, K. F.; Bawendi, M. G. *J. Phys. Chem. B* **1997**, *101*, 9463.

(8) Lee, Y. J.; Kim, T. G.; Sung, Y. M. *Nanotechnol.* **2006**, *17*, 3539.

(9) Alivisatos, A. P. *Science* **1996**, *271*, 933.

(10) Bruchez, M.; Moronne, M.; Gin, P.; Weiss, S.; Alivisatos, A. P. *Science* **1998**, *281*, 2013.

(11) Kwak, W. C.; Kim, T. G.; Chae, W. S.; Sung, Y. M. *Nanotechnol.* **2007**, *18*, 205702.

(12) Wong, E. M.; Bonevich, J. E.; Searson, P. C. *J. Phys. Chem. B* **1998**, *102*, 7770.

(13) Pesika, N. S.; Stebe, K. J.; Searson, P. C. *J. Phys. Chem. B.* **2003**, *107*, 10412.

(14) Huang, M. H.; Mao, S.; Feick, H.; Yan, H.; Wu, Y.; Kind, H.; Weber, E.; Russo, R.; Yang, P *Science* **2001**, *292*, 1897.

(15) Fukusima, M.; Managaki, N.; Fujii, M.; Yanagi, H.; Hayashi, S. *J. Appl. Phys.* **2005**, *98*, 024316.

(16) Okamoto, K.; Niki, I.; Shvartser, A.; Narukawa, Y.; Mukai, T.; Scherer, A. *Nat. Mater.* **2004**, *3*, 601.

(17) Hecker, N. E.; Höfel, R. A.; Sawaki, N.; Maier, T.; Stasser, G. *Appl. Phys. Lett.* **1999**, *75*, 1577.

(18) Wang, X.; Kong, X.; Yu, Y.; Zhang, H. *J. Phys. Chem. C* **2007**, *111*, 3836.

(19) Ma, G. H.; He, J.; Rajiv, K.; Tang, S. H.; Yang, Y.; Nogami, M. *Appl. Phys. Lett.* **2004**, *84*, 4684.

(20) Lin, H. Y.; Chen, Y. F.; Wu, J. G.; Wang, D. I.; Chen, C. C. *Appl. Phys. Lett.* **2006**, *88*, 16191.

(21) Mishra, Y. K.; Mohapatra, S.; Singhal, R.; Avasthi, D. K.; Agarwal, D. C.; Ogale, S. B. *Appl. Phys. Lett.* **2008**, *92*, 043107.

(22) Murphy, C. J.; San, T. K.; Gole, A. M.; Orendorff, C. J.; Gao, J. X.; Gou, L.; Hunydi, S. E.; Li, T. *J. Phys. Chem. B* **2005**, *109*, 13857.

(23) Wu, C.; Chen, J.; Wang, H.; Tan, F.; Li, S.; Qiao, X. *Mater. Lett.* **2006**, *60*, 1828.

(24) Lee, W. J.; Shi, E. W.; Zhong, W. Z.; Yin, Z. W. *J. Cryst. Growth.* **1999**, *203*, 186.

(25) Yguerabide, J.; Yguerabide, E. E. *Anal. Biochem.* **1998**, *262*, 137.

(26) Vanheusden, K.; Warren, W. L.; Seager, C. H.; Tallant, D. R.; Voigt, J. A.; Gnade, B. E. *J. Appl. Phys.* **1996**, *79*, 7983.

(27) Rayleigh, L. *Phil. Mag.* **1891**, *41*, 107.

(28) Rayleigh, L. *Phil. Mag.* **1891**, *41*, 274.

(29) Dijken, A. V.; Meulenkamp, E. A.; Vanmaekelbergh, D.; Meijerink, A *J. Phys. Chem. B* **2000**, *104*, 1715.

JP8018809